Effects of bedrock landslides on cosmogenically determined erosion rates

Nathan A. Niemi [a],[*], Michael Oskin [b], Douglas W. Burbank [a],[1],
Arjun M. Heimsath [c], Emmanuel J. Gabet [d]

[a]Institute for Crustal Studies, University of California, Santa Barbara, CA 93106, USA
[b]Department of Geological Sciences, University of North Carolina, Chapel Hill, NC 27599, USA
[c]Department of Earth Sciences, Dartmouth College, Hanover, NH 03755, USA
[d]Department of Geology, University of Montana, Missoula, MT 59812, USA

Abstract

The successful quantification of long-term erosion rates underpins our understanding of landscape formation, the topographic evolution of mountain ranges, and the mass balance within active orogens. The measurement of in situ produced cosmogenic radionuclides (CRNs) in fluvial and alluvial sediments is perhaps the method with the greatest ability to provide such long-term erosion rates. Although deep-seated bedrock landsliding is an important erosional process in active orogens, its effect on CRN-derived erosion rates is largely unquantified. We present a numerical simulation of cosmogenic nuclide production and distribution in landslide-dominated catchments to address the effect of bedrock landsliding on erosion rates. Results of the simulation indicate that the temporal stability of erosion rates determined from CRN concentrations in sediment decreases with increased ratios of landsliding to bedrock weathering rates within a given catchment area, and that as the frequency of landsliding increases, larger catchment areas must be sampled in order to accurately evaluate long-term erosion rates. In addition, results of this simulation suggest that sediment sampling for CRNs is the appropriate method for determining long-term erosion rates in regions dominated by mass-wasting processes, whereas bedrock surface sampling for CRNs may generally underestimate long-term erosion rates. Response times of CRN concentrations to changes in erosion rate indicate that climatically driven cycles of erosion may be detected, but that complete equilibration of CRN concentrations to new erosional conditions may take tens of thousands of years. Comparison of simulated CRN-derived erosion

* Corresponding author. Also at: Division of Geological and Planetary Sciences, California Institute of Technology, Pasadena, CA 91125, USA. Tel.: +1 626 395 6166; fax: +1 626 683 0621.
  E-mail addresses: niemi@gps.caltech.edu (N.A. Niemi), oskin@email.unc.edu (M. Oskin), burbank@crustal.ucsb.edu (D.W. Burbank), arjun.heimsath@dartmouth.edu (A.M. Heimsath), manny.gabet@mso.umt.edu (E.J. Gabet).
  [1] Also at: Department of Geological Sciences, University of California, Santa Barbara, CA 93106, USA.

rates with a new data set of such rates from the Nepalese Himalaya underscore the conclusions drawn from the model results.

1. Introduction

Observed changes in long-term erosion rates are often considered proxies for changes in the climatic or tectonic boundary conditions that control landscape evolution [1]. The measurement of in situ produced cosmogenic radionuclides (CRNs) in fluvial and alluvial sediments has been shown to yield spatially averaged erosion rates and has become perhaps the method with the greatest applicability in measuring erosion rates over 10^3–10^5 yr and across a wide variety of landscapes and erosional processes [2–6]. Most existing studies that utilize CRN-derived erosion rates have focused on regions with rather extensive spatially and temporally homogeneous erosion rates. Here we present a simulation to explore the effects of bedrock landsliding on cosmogenic erosion rates and the poten-

tial for exploiting cosmogenic nuclides to measure erosion rates in rapidly eroding, active orogens.

Large bedrock landslides can incise to depths greater than the attenuation length of cosmic rays, thus mobilizing sediments with little or no cosmogenic nuclide abundance (Fig. 1). Based on empirical relationships of landslide depth to area [7], a landslide with a radius of just 10 m will incise to ~100 cm, below the attenuation length of spallogenic nuclide production. An extraordinarily large slide may incise to a maximum depth of several tens of meters, below the attenuation length of muogenic nuclide production. In catchments where deep landslides have recently occurred, the addition of nuclide-poor landslide detritus to the fluvial system will dilute the CRN concentration in the fluvial sediment, yielding apparently higher erosion rates. As one example, samples
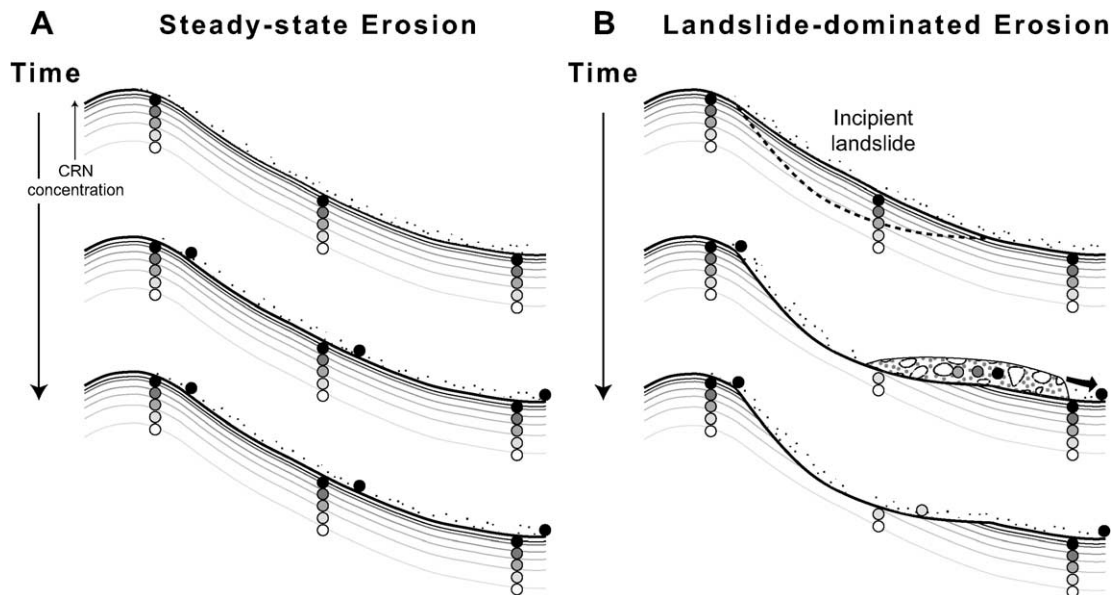

Fig. 1. Cartoon showing the effects of landslides on surface cosmogenic nuclide concentrations and indicating particle paths during erosion. (A) Homogeneous CRN surface concentration and sediment volume and concentration during steady-state erosion. (B) Heterogeneous surface CRN concentration and heterogeneous sediment volume and CRN concentration during landslide-dominated erosion.

from low-order fluvial catchments in the Nepalese Himalaya yield 'erosion rates' determined from cosmogenic nuclides that range from 0.01 to 0.4 mm/yr, even along the same ridge crest ([8,9]; Heimsath et al., in preparation). Similar results are reported from the San Bernardino Mountains in southern California, where 'erosion rates' along a landslide-dominated escarpment vary from <0.3 to >2.7 mm/yr, while rates from an adjacent region dominated by bedrock weathering are on the order of hundredths of millimeters per year [10].

Such variability may be expected for data sets that are focused on small, steep catchments in actively deforming mountain belts, but it complicates the application of in situ produced CRNs in interpreting the rates of erosion in regions affected by both bedrock weathering and landsliding processes.

Here we address the effects of bedrock landsliding on CRN-derived erosion rates from bedrock and fluvial samples in an attempt to answer several basic questions: As the rate of landsliding increases, how are CRN concentrations in fluvial sediment affected? Can reliable CRN erosion rates be derived from fluvial sediment or bedrock samples when landsliding is the dominant erosional process? Over what spatial scales do fluvial systems integrate the effects of landsliding? What timescales are required for CRN concentrations to respond to changes in erosion rates? We present the results of a numerical simulation of cosmogenic nuclide production and erosional removal in landslide-dominated catchments to assess these questions. A series of simulations with varying bedrock weathering and landslide erosion rates are used to create statistical populations of CRN-derived erosion rates for both 'sediment' and 'bedrock' samples for a theoretical landscape. Finally, simulated distributions of CRN-derived ages are compared to a new, extensive data set of CRN-derived erosion rates from the Nepalese Himalaya.

2. Numerical simulation

The numerical simulation is based on actual digital elevation data, and it simulates the production of cosmogenic nuclides at each model cell, the removal of material through bedrock weathering, the removal of material by landsliding, and the radioactive decay

of cosmogenic nuclides. A Geographic Information System (GIS; in this case ArcInfo) is used for the backbone of the simulation. Model initialization, data assimilation, and data output are all controlled through the GIS using Arc Macro Language (AML). Computationally intensive portions of the model are passed from the GIS to customized Perl modules for computational efficiency. The three main functionalities of the simulation are described in greater detail below.

2.1. Cosmogenic nuclide production

Prior to running the landslide simulation model, cosmogenic nuclide production rates must be calculated for each cell in the model. Calculation of these rates begins with a geo-referenced digital elevation model (DEM) of the study area of interest. For each cell in the digital elevation model, cosmogenic production scaling factors are calculated within the GIS based on cell altitude and latitude following [11,12]. Further corrections to cosmogenic production are applied by calculating the topographic shielding at each point in the DEM. For each cell in the DEM, the vertical angle to every other cell is calculated. These values are binned into $5°$ radial bins, and the maximum vertical angle in each bin is used to approximate the horizon angle for that bin. The topographic shielding factor for each bin is derived from the horizon angle using a published methodology [13]. The altitude, latitude, and topographic shielding factors are combined within the GIS system to produce an output array of cosmogenic production scaling factors. This array is then multiplied by the high-latitude, sea-level production rate of the cosmogenic nuclide of interest to create an array of cosmogenic production rates. In this case, we have chosen to model ^{10}Be and selected a production rate of 5.3 atoms/g/yr [14]. This array of ^{10}Be production rates is preserved for use through the rest of the model run.

2.2. Model initialization

Model initialization consists of two separate actions: (i) preparing the model for data gathering and assimilation and (ii) calculating an initial surface cosmogenic nuclide concentration to start the landslide model. The first of these two tasks is the most time-intensive and must be performed separately for

each DEM on which this model is run. Using the hydrologic functions available in a GIS, watersheds within the model area are delineated. A variety of first- to highest order watersheds are selected and saved for later use in data analysis. One hundred random points are also generated across the model space at which to track cosmogenic nuclide concentrations in bedrock and erosional removal of material. This number of points was chosen as the minimum number of points that adequately represent the distribution of erosion rates across the landscape. After the data gathering initialization steps are complete, an input cosmogenic surface nuclide concentration array must be calculated for input to the landslide portion of the model. We have chosen to input a surface concentration grid that represents the steady-state concentration of ^{10}Be at the bedrock weathering rate specified for the model run. The bedrock weathering rate is limited by the rate at which rock can be converted to soil or regolith and is taken to be less than 0.3 mm/yr [15]. The surface concentration (N) is calculated for each point in the model following the equation

$$N^{10}\text{Be} = \frac{P^{10}\text{Be}}{\left(\lambda_{10\text{Be}} + E/\Lambda\right)} \left(1 - e^{-\left(\lambda_{10\text{Be}} + E/\Lambda\right)t\right)}, \quad (1)$$

where $N^{10}\text{Be}$ and $P^{10}\text{Be}$ are the concentration (atoms/ g) and production rate (atoms/g/yr) of ^{10}Be, respectively; $\lambda_{10\text{Be}}$ is the decay constant of ^{10}Be (yr^{-1}); E is the erosion rate (here equivalent to the bedrock weathering rate), in g/cm^2/yr; Λ is the neutron attenuation length in rock, in g/cm^2; and t is time (yr). This initial concentration array is saved for input into future model runs.

2.3. Landslide simulation

The landslide simulation portion of the model takes as input the surface cosmogenic nuclide concentration array calculated in the previous step, and the cosmogenic production rate array calculated in the first model step. This portion of the model is iterated. At the end of each iteration, two arrays are output, a depth array which contains the sum of all sediment removed by erosion, due to both bedrock weathering and landsliding, and a surface concentration array that contains the surface cosmogenic nuclide concentration at each model cell after erosional removal of

material, cosmogenic ingrowth and radioactive decay. The individual steps are detailed below.

2.3.1. Cosmogenic ingrowth and decay

Given an initial surface cosmogenic nuclide concentration, $N_i^{10}\text{Be}$, and a surface cosmogenic nuclide production rate, $P^{10}\text{Be}$, a resultant surface cosmogenic nuclide concentration, $N_r^{10}\text{Be}$, produced by cosmic ray bombardment and removal by radioactive decay can be calculated by

$$N_r^{10}\text{Be} = \left(N_i^{10}\text{Be} + P^{10}\text{Be} \cdot t\right) e^{-\lambda_{10\text{Be}}t}. \quad (2)$$

The new surface concentration, $N_r^{10}\text{Be}$, replaces the initial value in the surface concentration array.

2.3.2. Bedrock weathering

The bedrock weathering rate (E_b) represents the spatially homogeneous erosional removal of material from the land surface. For each model time step (t), a depth equal to $E_b \times t$ is added to the depth grid. This material is always removed from the upper surface of the topography and therefore has the highest concentration of CRNs.

2.3.3. Landslides

After removal of material by bedrock weathering, the model is populated with landslides. Landslides are assumed to obey a power-law frequency–magnitude relationship [7,16–23]. Based on this assumption, populations of landslides in the model can be derived from four parameters: β, the power-law exponent for landslide frequency–magnitude relationship, $A_{\min}$, the minimum landslide area, $A_{\max}$, the maximum land- slide area, and E_{ls}, the average rate of erosion by landsliding over the model area. Although short-term landslide erosion rates fluctuate due to the episodicity of landslides, the average rate of erosion by land- sliding is produced through the power-law fre- quency–magnitude relationship over time (Fig. 2). Complete derivations of landslide frequency–magni- tude distributions in the model space are given in Appendix A. For each model timestep, a landslide distribution is generated, and the landslides are ran- domly distributed over the model space. The total amount of material removed by landsliding from each model cell during the timestep is then calculated. The total depth of material removed by landsliding is
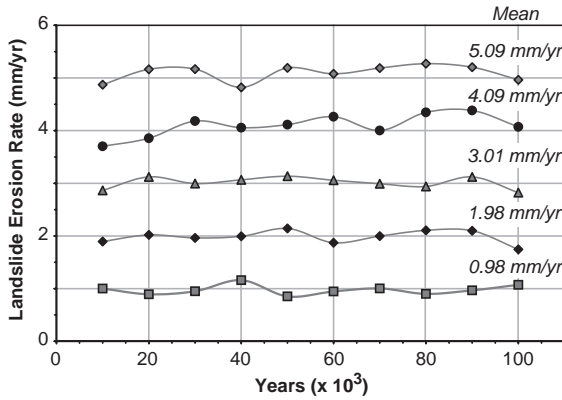
Fig. 2. Comparison of output model landslide erosion rates with prescribed landslide erosion rates, averaged over 10,000-yr time steps. Mean erosion rates for the 100,000-yr model run are shown at the right of the figure. Short-term variations in landslide erosion rate are due to random distribution of slide size; long-term landslide erosion rates return input erosion rates $\pm 3\%$.

added to the depth of material removed by bedrock weathering (see Appendix A).

2.3.4. Surface concentration

Once the depth array is tabulated, the surface cosmogenic nuclide concentration is recalculated to reflect the depth of material removed from each model cell. Assuming, for simplification, a constant rock density (ρ) in the model of 2.65 g/cm^3, and a cosmogenic ray attenuation length in this rock (Λ) of 150 cm^2/g, a final surface cosmogenic nuclide concentration at the end of the timestep, N_f^{10}Be, can be calculated for each cell based on the cosmogenic concentration following ingrowth, N_r^{10}Be, above, and the depth of material, D, removed from the cell during the timestep,

$$N_f^{10}\text{Be} = N_r^{10}\text{Be} \cdot e^{-D(\rho/\Lambda)}. \tag{3}$$

The value N_f^{10}Be is stored for each cell in the surface concentration array. At this point, this array is saved for data extraction, as described in the next section, and then re-opened as the initial surface concentration grid for the next iteration step of the landslide portion of the model.

2.4. Data extraction

At a specified sampling interval, data are extracted from each array to simulate two potential cosmogenic

nuclide sampling methods: surface exposure age dating and stream sediment sampling.

2.4.1. Surface exposure age dating

The depth of material removed and the final surface concentration at each sample point across the model are recorded. A volumetric erosion rate (E_v) is calculated by dividing the depth of material removed (D) by the model time step (t; recall that D includes both continual removal of rock by bedrock weathering and episodic landsliding). Additionally, a cosmogenic erosion rate (E_c) is calculated for each point using the standard assumption of steady-state erosion [24],

$$E_c = \frac{\Lambda}{\rho} \left(\frac{P^{10}\text{Be}}{N_f^{10}\text{Be}} - \lambda_{^{10}\text{Be}} \right). \tag{4}$$

2.4.2. Stream sediment sampling

Cosmogenic nuclide concentrations in stream sediments can be used to estimate average upstream erosion rates of watersheds. For each watershed, a volumetric erosion rate (E_v) is calculated by summing the total depth of material removed from the watershed and dividing it by the watershed area multiplied by the model time step. Second, a cosmogenic erosion rate (E_c) for the watershed is calculated. To calculate this erosion rate, first, the concentration of the cosmogenic nuclide of interest in the eroded sediment must be determined. Using the depth array and surface concentration array, the average nuclide concentration in the eroded material at each model cell, N_D^{10}Be, can be calculated as

$$N_D^{10}\text{Be} = N_f^{10}\text{Be} \cdot \Lambda \left(1 - e^{D(\rho/\Lambda)} \right). \tag{5}$$

The concentration of cosmogenic nuclides in the sediment removed from the watershed, N_S^{10}Be, then, is

$$N_S^{10}\text{Be} = \sum N_D^{10}\text{Be} \bigg/ \sum D. \tag{6}$$

The erosion rate derived from the cosmogenic nuclide concentration in the material removed from the watershed is then calculated as in Eq. (4), where P^{10}Be would represent the watershed-averaged production rate and N_f^{10}Be would be replaced with N_S^{10}Be.

2.4.3. Simplifications and assumptions

It should be noted that the model outlined above makes several simplifying assumptions regarding sediment production and transport. Bedrock weathering and transport is assumed to occur at a homogeneous rate across the entire model, although in reality, the rate at which these processes act on the scale of our model are controlled by local slope and lithology. Landslides are also randomly placed across the landscape, with no considerations for hillslope and aspect. Second, the model contains no provision for sediment storage. All material derived from landsliding is assumed to pass through the model within the timestep in which the landslide occurred (100 yr for the models discussed here). Third, the model is intended to produce a population of cosmogenic and volumetric erosion rates for statistical analysis. Erosion and landslides occur through 'time' to produce a variety of surface CRN concentrations that could potentially be sampled; however, this model is not a landscape evolution model. During the course of the model run, the model landscape surface does not evolve, and shielding effects or absolute elevation changes that in reality would alter CRN production rates are not considered. Finally, the role of muogenic production is not explicitly considered in this simulation. The greater attenuation length of muons results in larger proportion of muogenic to spallogenic nuclide production at higher erosion rates [25], such as those considered in this model, and thus, our modeled cosmogenic erosion rates immediately following a landslide may be considered maximum estimates. On the other hand, extremely large landslides may incise well below the attenuation length of muogenic production, negating this effect. The frequency of such large events will dictate the effects of considering muogenic production on our model results.

3. Model results

We simulated the effects of landsliding on cosmogenic nuclide equilibrium and associated CRN-derived and volumetrically calculated erosion rates for the San Antonio Creek catchment, located in the eastern San Gabriel Mountains of southern California (Fig. 3). It is a small (~70 km^2), mountainous catchment, selected in part because of the availability of
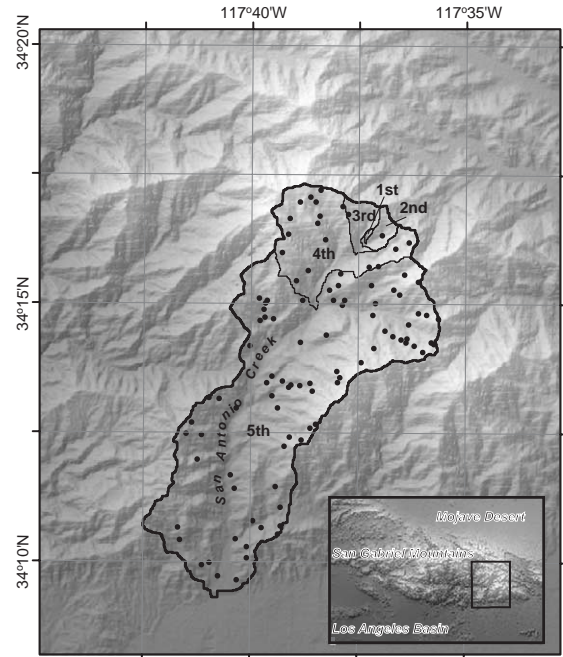

Fig. 3. Shaded relief map of the San Antonio Creek watershed, San Gabriel Mountains, California. The full watershed is outlined with a heavy black line, while representative smaller order watersheds are indicated with a lighter black line. Random 'bedrock' sampling points (discussed in the text) are shown as black dots.

high-quality digital elevation model (DEM) data over the region (30-m resolution), and in part because a significant amount of work exists describing the geomorphology and neotectonics of the region. Low-temperature thermochronologic data indicate that the eastern San Gabriel Mountains are being exhumed at a rate of ~0.3–1 mm/yr [26–28], while geomorphic and geologic studies indicate that landsliding is a prevalent mechanism of erosion in this watershed [17,29]. In fact, both a landslide frequency–magnitude exponential scaling factor (β) and a long-term average erosion rate have been determined for this region [17]. When β is less than 1.5, large, but infrequent landslides dominate the overall sediment flux from a catchment. As such, this watershed potentially provides a natural laboratory to study the effects of landsliding on CRN-derived erosion rates, and for comparison with and calibration of the numerical model.

The San Antonio Creek watershed was divided into 46 sub-basins that were tracked as part of this

Table 1
Statistics for basins tracked in the model

Basin order	Number of basins	Mean area (km^2)
First	30	0.1
Second	6	0.6
Third	5	2.3
Fourth	4	8.4
Fifth	1	69.0

simulation, and from which modeled sediment-derived CRN erosion rates were calculated (examples shown in Fig. 3; basin statistics are listed in Table 1). In addition to the sub-basins, 100 points were randomly distributed across the model space to serve as simulated bedrock CRN sampling localities (Fig. 3). Modeled bedrock weathering rates were selected that span the range of observed bedrock weathering rates in the Transverse Ranges [10] to the most rapid known rates of rock-to-regolith conversion [15]. Landslide parameters used were $\beta = 1.18$ [17], $A_{min} = 30$ m, the input DEM cell size, and $A_{max} = 1000$ m, the maximum local topographic relief. Nine model runs were completed with various combinations of bedrock weathering, landslide, and total erosion rates (Table 2). Each model ran for 100,000 yr with a 100-yr timestep, and CRN concentrations were recorded every 1000 yr. Simulation results are summarized on a box-and-whisker plot (Fig. 4).

3.1. Simulated sediment erosion rates

Catchment-wide erosion rates allow comparison of the statistical distributions between CRN-derived and volumetrically averaged erosion rates for each of the nine simulations and illustrate variations as a function of catchment order (Fig. 5).

Table 2
Landslide rates for each model run

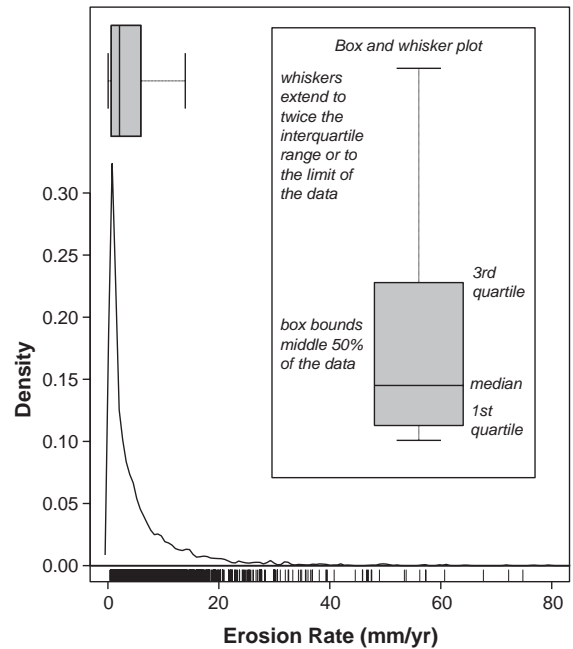| Total erosion rate	Bedrock weathering rate		
	0.01	0.1	0.3
1.0	0.99	0.90	0.70
5.0	4.99	4.90	4.70
10.0	9.99	9.90	9.70

All erosion rates are in mm/yr.

Fig. 4. Example of a box-and-whisker plot to graphically display the statistical distribution of a non-Gaussian data set. A probability density function (PDF) and box-plot are shown for actual model results of cosmogenic erosion rates from first-order basins with a bedrock weathering rate of 0.1 mm/yr and a total erosion rate of 10 mm/yr. The distribution of erosion rates is plotted across the bottom of the graph as a series of vertical black hash marks.

Several conclusions can be drawn from these data. First, with increasing proportion of bedrock weathering, the CRN-determined erosion rate at any catchment scale more closely reflects the volumetric erosion rate for any given total combined erosion rate (Fig. 6). This is not unexpected, as bedrock weathering is modeled as a uniformly continuous process in the simulation, such that increased ratios of bedrock weathering to landsliding will result in a greater contribution from a steady-state process to the overall erosional volume. It is worth noting that under this formulation, for any given total erosion rate, an increase in bedrock weathering rate results in a decrease in the rate of erosion due to landsliding. Thus, for a given basin size, CRN-derived erosion rates converge with volumetric erosion rates with an increase in the rate of bedrock weathering, but diverge from the total erosion rate due to the reduction in landsliding (Fig. 6). Additionally, the data emphasize that the observed magnitude–frequency
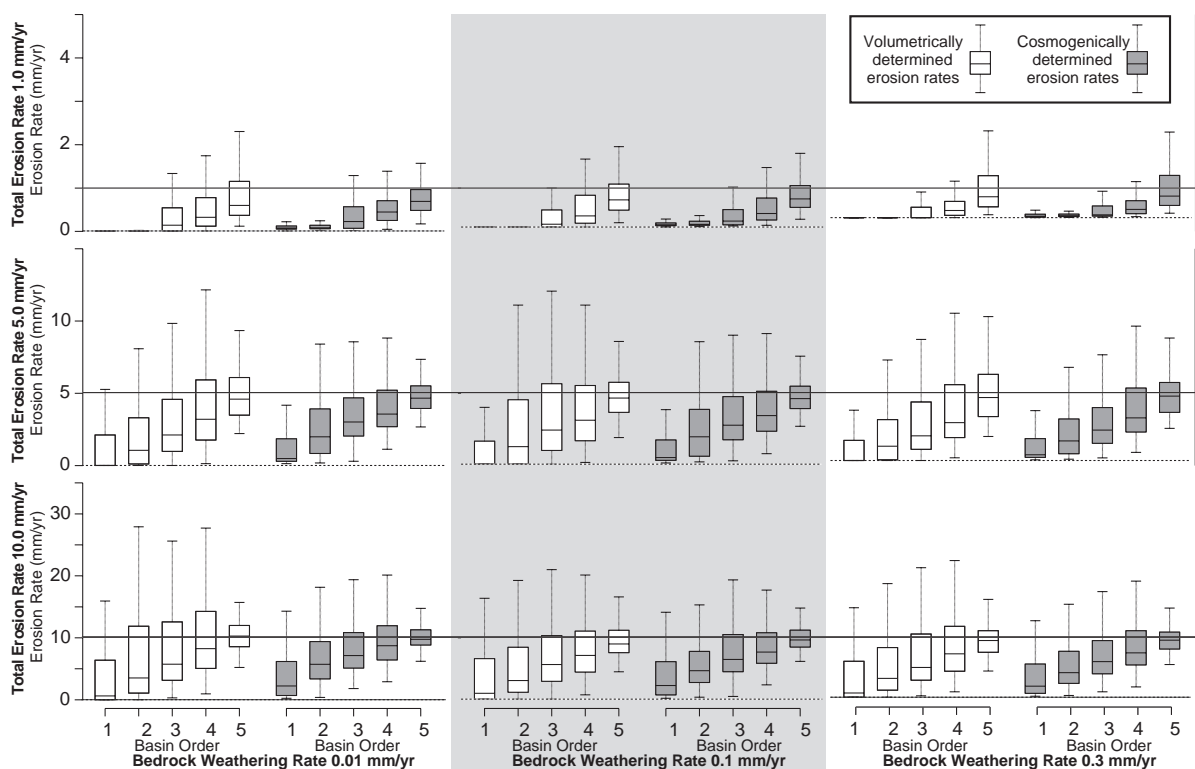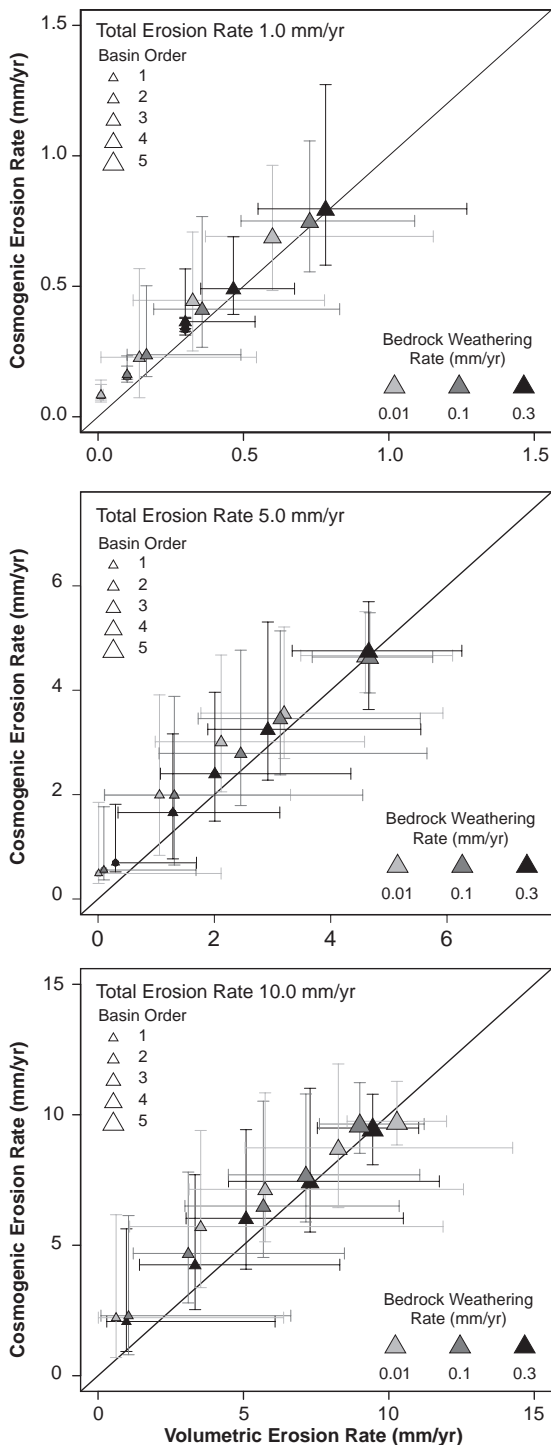
Fig. 5. Box-and-whisker plots of CRN-derived erosion rates and volumetric erosion rates for nine separate simulations with three combinations of bedrock weathering and total erosion rates. Upper solid line on each graph indicates total erosion rate; lower dashed line indicates bedrock weathering rate. See text for detailed discussion.

relationships of landslides skew volumetric erosion towards the larger, more infrequent, landslides [16,17]. This is reflected in all nine simulations, where the median 50% of the CRN-derived and volumetric erosion rates generally fall below the total imposed erosion rate in the simulation. The outer statistical bounds of the CRN-derived and volumetric erosion rates are substantially higher than the imposed erosion rates, reflecting the infrequency, but importance, of these large events in controlling erosion rates in landslide-dominated catchments.

The effects of damping and averaging effects on CRN-derived erosion rates are also illustrated in the statistical spread of the model data set (Fig. 5). Volumetric erosion rates display a greater spread than CRN-derived rates at all catchment scales, bedrock weathering rates, and landslide rates. These effects are particularly notable at small to moderate catchment scales in regions with low rates of ero-

sion by landsliding. In particular, at 1 mm/yr total erosion rate, the CRN-derived rates have a 50% smaller distribution than the volumetric erosion rates.

The effect of spatial averaging on the spread of volumetric- and CRN-derived erosion rates is also highlighted in our results (Fig. 5). The statistical spread of both volumetric erosion rates increases with increasing catchment size is presumably related to the increased likelihood of experiencing a large mass wasting at greater catchment area. Once an appropriate spatial threshold is reached, if the catchment becomes large enough to adequately average large landsliding events and areas unaffected by mass wasting, the spread of the erosion-rate data drops significantly. This spatial scale in our simulations appears to occur between fourth- and fifth-order catchments (a jump from ~8 km^2 to ~70 km^2). The exception to this rule is at low total erosion rates,

where landslides appear to occur infrequently enough at all catchment scales to never significantly decrease the statistical distribution of erosion rates from third- to fifth-order catchments.

Finally, given the damping and spatial averaging effects described above, it is heartening to note that the median 50% of observations are more or less consistent between volumetric and CRN-derived erosion rates (Fig. 5). At small catchment scales, CRN-derived rates are typically higher than volumetric rates (this is particularly clear at low total erosion rates), but converge at larger catchment scales (Fig. 6). The catchment size at which this convergence occurs varies and decreases with increased rates of erosion. As a general rule of thumb, however, it would appear that CRN-derived rates of erosion from sediments are statistically representative of volumetric rates in our numerical simulation at third-, or at most, fourth-order catchment scales. This observation indicates that CRN-derived erosion rates from sediments in landslide-dominated catchments may in fact be useful for looking at basin-wide erosion at intermediate time scales (10^3–10^4 yr) to study the variability of spatial and temporal distributions of landsliding. Measuring CRN-derived erosion rates from several third- or fourth-order catchments should allow the identification of high erosion rates that may be due to recent mass wasting events. Such high rates would approximate the recent volumetric erosion rates from the basin, but not necessarily the long-term average (Fig. 5). However, even catchments as large as the fourth-order catchments in our study are likely to underestimate the overall erosion rate by 20–40%, due to the impact of rare, but unusually large, landslide events. The impact of such events is only averaged at the largest catchment scale, where the first to third quartiles of cosmogenic erosion rates overlap the long-term average rate, yielding an ~50% chance of determining a cosmogenic erosion rate within ~20% of the long-term average (Fig. 5).

Fig. 6. Scatter plots of median cosmogenic vs. median volumetric erosion rates for (from top to bottom) total erosion rates of 1, 5, and 10 mm/yr. All plots indicate that cosmogenic erosion rates are higher than volumetric erosion rates and illustrate the convergence of the two rates with increased bedrock weathering rate. Error bars as in Fig. 5.

3.2. Simulated bedrock erosion rates

We also calculated the surface CRN concentration at 100 points as though bedrock samples were collected from each of these locations (Eq. (4); Fig. 7).

A first-order observation is that the spread of erosion rates increases with increasing rates of total erosion and, thus, with increasing rates of landsliding. This almost certainly reflects the increased likelihood that any of the randomly sampled points in the model will be affected by landsliding with the increasing frequency of events. A second important observation is that at low rates of total erosion (and landsliding), although bedrock weathering encompasses, at most, 30% of total erosion, the median CRN-derived erosion rate is almost identical to the bedrock weathering rate. That is, for any given point in the landscape, the likelihood of sampling a point that has been recently enough affected by mass wasting to alter the CRN concentration is virtually negligible. As the total rate of erosion increases, the median erosion rates increase above the background bedrock weathering rate, yet fall well below the total erosion rate over the landscape. In contrast to the distribution of sediment-derived CRN erosion rates (Fig. 5), the upper extent of the 'whisker' (three inter-quartile ranges beyond the median) never exceeds the imposed total erosion rate. In fact, the highest percentage of 'bedrock' samples that accurately reflect the total erosion

rate is 0.25%, for the model run with a total erosion rate of 10 mm/yr and a bedrock weathering rate of 0.01 mm/yr, where 25 samples out of 10,000 fell within the range of 8–12 mm/yr.

These results suggest that sampling bedrock exposures in basins dominated by mass wasting may provide an upper bound on bedrock weathering rates across the basin but are likely to underestimate the long-term rate of erosion resulting from the combined effects of bedrock weathering and landsliding.

3.3. Response of CRN-derived erosion rates to changes in rates of mass wasting processes

Whereas the calculation of CRN and volumetric erosion rates is only performed while the simulation is in an erosional 'steady state' for the imposed landslide and bedrock weathering rates, the mean CRN concentration is calculated throughout the model run to gather an estimate of the response time of CRNs in the landscape to changes in erosional boundary conditions (Fig. 8). These plots record the mean [10]Be concentration over the landscape, beginning at the initialization of the model, where the [10]Be concentration at each cell in the simulation is analytically solved for the imposed bedrock weathering rate and the scaled production factor at each cell. Subsequently, landslides are populated across the model landscape, and the mean concentration of [10]Be begins to decrease at a rate controlled by the bedrock weath-
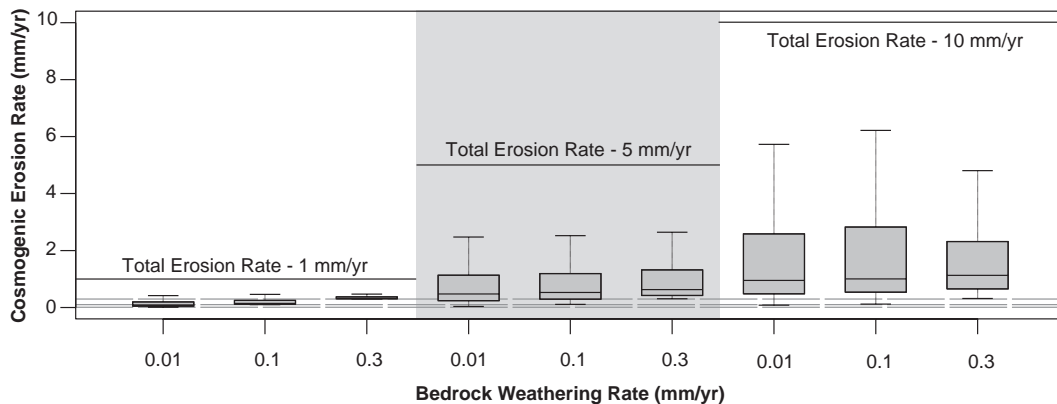

Fig. 7. Distribution of cosmogenically determined erosion rates (shaded boxes) from individual sample points for each model run. Total erosion rates for each set of runs are indicated by solid lines; bedrock weathering rates are drawn across the lower portion of the graph in dashed lines. As landslide erosion rates increase, the spread and median of cosmogenically derived erosion rates also increase. Median cosmogenically determined erosion rates at these points, however, remain well below total erosion rates for each model run.
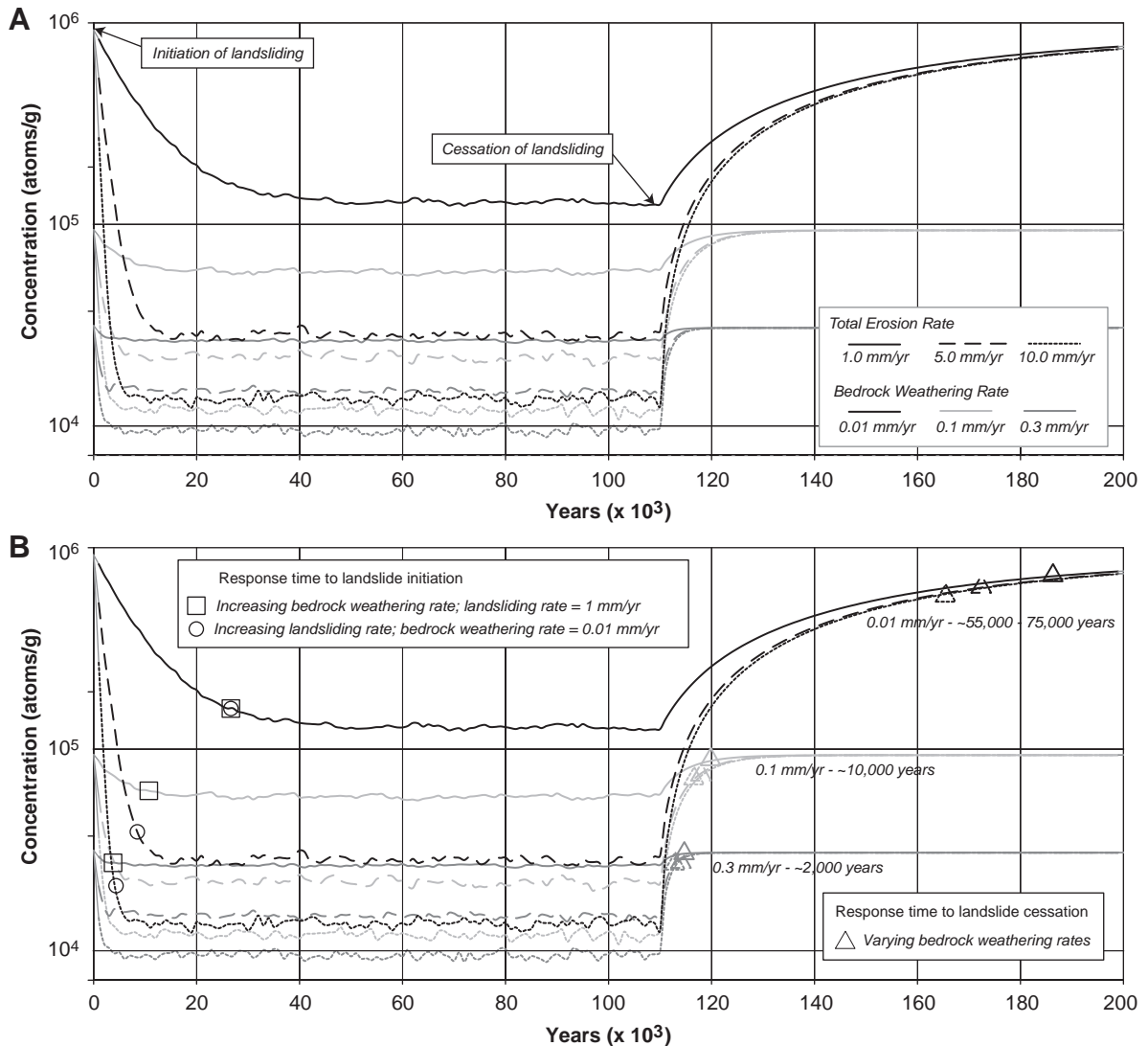
Fig. 8. Mean concentration of [10]Be across the simulation, showing the effect of initiation and cessation of landslides on [10]Be concentration at several different rates of bedrock weathering and landsliding. (A) Mean [10]Be concentration through time for all model runs; initiation and cessation of landsliding indicated. (B) Symbols highlighting variation in response time to changing boundary conditions, see text for discussion.

ering rate and the total rate of landsliding imposed on the model. After a period when mean [10]Be concentration steady-state is achieved during bedrock weathering and landsliding, the landslides are eliminated from the simulation, and the mean [10]Be concentration in the landscape increases (Fig. 8A).

Tracking of specific points emphasizes the effects of changes in bedrock weathering and landsliding

rates on the response time of mean [10]Be concentration (Fig. 8B). The response time of the landscape to achieve a new equilibrium mean [10]Be concentration is a function of both the bedrock weathering rate and the landsliding rate. For a given total erosion or bedrock weathering rate, the time for [10]Be to reach a new equilibrium decreases with an increase in the other rate. Increasing the bedrock weathering rate by a

factor of 10 decreases the time necessary for [10]Be to reach a new equilibrium concentration (squares on Fig. 8B); likewise, increasing the rate of landsliding by a factor of 5 also yields a decrease in the response time (circles on Fig. 8B). On the other hand, when landsliding is absent, the response time for re-equilibration of mean [10]Be concentration is a function solely of the bedrock weathering rate. The time necessary for a landscape to recover 95% of its pre-landslide mean [10]Be concentration is as little as 2000 yr, at bedrock weathering rates of 0.3 mm/yr, and as great as 55,000 to 75,000 yr at bedrock weathering rates of 0.01 mm/yr (triangles on Fig. 8B).

These results indicate that in rapidly eroding landscapes, alternating between landsliding and non-landsliding erosional regimes over relatively short time periods (less than a few thousand years) may generate transients in CRN concentrations lasting tens of thousands of years. If landsliding is a more prevalent mechanism of erosion under certain climatic regimes (e.g., during interglacial periods; [30–32]), then the response time of mean [10]Be concentration to changes in landsliding rate must be considered.

4. Comparison of simulation results of CRN erosion rates to CRN erosion rates from the Nepalese Himalaya

The Khudi River in Nepal, a tributary to the Marsyandi River, has been the focus of a multi-disciplinary study of geomorphic and geodynamic coupling in the Himalaya [33,34]. As part of this study, erosion rates over this catchment have been assessed using a variety of techniques, including long-term erosion rates from low-temperature thermochronometers ($\geq$ 2–5 mm/yr; [33]), and present-day erosion rates (~3.7 mm/yr) from suspended sediment load (~2.5 mm/yr, E. Gabet, unpublished data) and bedload ratio determinations (2:1 ratio of suspended load to bedload, or 1.2 mm/yr; [35]). In addition, [10]Be CRN erosion rate determinations were made throughout the catchment, both from bedrock exposures and zero-order ($\leq$ 0.01 km^2) catchments, and from the mouth of the Khudi River (catchment size ~131 km^2) where it joins the Marsyandi River ([8,9]; Heimsath et al., in preparation). The measured CRN erosion rates were calculated using the same production rates

and scaling factors as in the model and have an average error of 10%. Here we compare the statistical distribution of 41 [10]Be CRN erosion rate determinations from bedrock exposures and zero-order catchments with predicted statistical distributions of CRN erosion rates determined from our simulation. Additionally, we calculate distributions of CRN erosion rates predicted at the mouth of the Khudi River and compare these with the basin-wide CRN erosion rates determined for the Khudi catchment.

The simulation of landsliding, cosmogenic production, and erosion was performed as described for the theoretical study in the San Antonio Creek watershed, with only a few modifications. First, the highest resolution DEM available for Nepal has ~90-m cell spacing, as opposed to the 30-m spacing available for San Antonio Creek. Therefore, the smallest landslide populated in the model was adjusted to have a radius of 90 m. Second, available erosion rate data from thermochronologic and sediment-load studies were used to establish a range of landsliding rates to input to the model of the Khudi catchment. A bedrock weathering rate of 0.15 mm/yr was assumed for the initial model runs, and landsliding rates of 2.85, 3.35, and 3.85 mm/yr (for total erosion rates of 3, 3.5, and 4 mm/yr) were selected. The best fit run was then re-analyzed with varying bedrock weathering rates to derive a statistical distribution of bedrock and small-order catchment CRN erosion rates for comparison with existing CRN data. Finally, the size of the zero- and first-order catchments is of order the size of the model cell spacing, so these small catchments were treated as points within this model.

4.1. Detrital CRN erosion rate in the Khudi catchment

The distribution of CRN erosion rates derived from the model for the entire Khudi drainage were compared with a [10]Be-derived erosion rate measured on sediment deposited at the mouth of the Khudi River. The measured CRN erosion rate of 3.4 ± 0.3 mm/yr best matches the model run with a total erosion rate of 3.5 mm/yr (0.15 mm/yr bedrock weathering and 3.35 mm/yr landslides; Fig. 9A). This result supports the theoretical determination that at high landslide erosion rates, the effects of landsliding on CRN erosion rates should be spatially
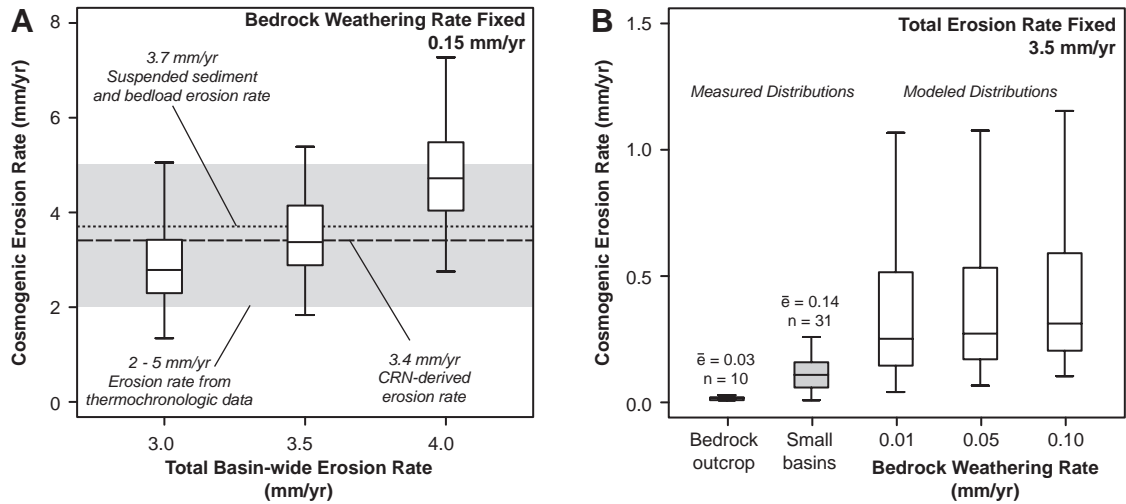
Fig. 9. (A) Distribution of model basin-wide CRN-derived erosion rates from the mouth of the Khudi drainage for erosion rates of 3.0, 3.5, and 4.0 mm/yr. The dashed line is the measured [10]Be erosion rate of 3.4 mm/yr from the mouth of the Khudi River [8,9]; the dotted line is the suspended sediment and bedload derived erosion rate (E. Gabet, unpublished data; [35]), and the gray box is the range of erosion rates from thermochronologic data [33]. (B) Comparison of simulated distributions of CRN-derived erosion rates from 41 sample locations (white boxes) where actual CRN-erosion rates were measured (gray boxes; A. Heimsath, unpublished data) for bedrock samples in zero- and first-order catchments in the Khudi drainage. Median CRN erosion rates for both the simulated data and the actual CRN data are an order of magnitude less than the basin-wide erosion rate (A).

averaged over large catchments, and that CRN methods are an effective means of assessing average erosion rates. Further, the median values of each of these three model runs does not overlap the first to third quartiles of any other run (Fig. 9A), indicating that the medians of these model runs statistically differ [36]. The results of this simulation, in concert with the actual CRN erosion rate, allow a determination of the erosion rate in the Khudi catchment of 3.5 ± 0.5 mm/yr, tightening the constraints on the erosion rate as derived from thermochronologic and sediment-load data.

4.2. Bedrock and small-order catchment CRN erosion rates in the Khudi catchment

Using the total erosion rate of 3.5 mm/yr determined for the entire Khudi drainage basin, three additional model runs were executed at increasing rates of bedrock weathering (0.01, 0.05, and 0.10 mm/yr) to compare the simulated distributions of CRN erosion rates with the distribution of CRN erosion rates determined from 41 [10]Be erosion rates for bedrock samples ($n=10$) and from zero- and first-order catchments ($n=31$; Heimsath et al., in

preparation; Fig. 9B). In the model space, the same 41 locations that were actually sampled were used to determine a theoretical distribution of erosion rates. Because the zero- and first-order catchments are of the order of the cell size of the model (~90 m), both bedrock and small-order basin samples were treated as point samples in the model run.

4.2.1. CRN erosion rates from small catchments

The comparison of measured CRN-derived erosion rates from small catchments with model results indicates that sampling small drainage basins for CRN concentrations in regions with significant erosion by bedrock landsliding is not an effective approach to determining the spatially and temporally averaged erosion rate over the encompassing larger drainage basin. The CRN data set from the Khudi drainage is one of the largest erosion rate data sets produced, yet the number of samples collected, and the percentage of the landscape that they represent, is inadequate to provide a meaningful representation of the erosion rate over the entire Khudi catchment, and, in fact, differ from the entire Khudi erosion rate by a factor of 25 (a median erosion rate of ~0.14 mm/yr in zero- and first-order catchments, compared with ~3.5

mm/yr across the entire Khudi basin). Interestingly, the distribution of measured CRN erosion rates from small catchments was significantly different from the modeled distribution of rates from the same catchments. The median measured erosion rate was a factor of two less than the median modeled rate, and the spread of measured rates was a quarter the spread of the modeled rates (Fig. 9B). One possible explanation for this difference stems from the sampling strategy employed in the Khudi study. Due to the steepness of the topography in the Khudi drainage, most detrital samples were collected from small basins right along major ridge crests. In our simulation, landslides in the model space are placed randomly, such that a ridge crest is just as likely to be affected by landsliding as a hillslope. In reality, this is not likely to be the case. Landslide mapping indicates that although landslides are preferentially located in areas of steep slopes near the headwaters of drainage systems, such slides rarely breach the drainage divide and lower the interfluve (e.g., [37]). Lowering of drainage divides occurs during infrequent events when the topographic slope below the ridge crest has been oversteepened by repeated landsliding, and landslide failure cuts under the drainage divide, removing the ridge crest. This process is likely to be highly undersampled, and the lower erosion rates and condensed spread of measured erosion rates along the ridge crests of the Khudi basin may reflect this fact. A slight increase in measured erosion rate with distance from the ridge crest for small catchments also hints that this explanation is a plausible one, but the number of samples available is insufficient for a rigorous analysis of this effect.

4.2.2. CRN erosion rates from bedrock samples

CRN samples collected from bedrock outcrops display an even lower median erosion rate and overall spread of rates than the detrital samples collected from the small catchments. As with the detrital samples, the bedrock samples in the Khudi drainage were collected along the ridge crest. Samples that were judged to not have been recently affected by landsliding were specifically targeted. As such, the spread of CRN ages would be expected to be smaller than a truly random set of ridge crest samples, and the median erosion rate would, as a result, be lower than a truly random sampling transect. This effect notwithstanding, the

median erosion rates from the bedrock samples are still surprisingly low; nearly a factor of 5 lower than the detrital samples from the same region (Fig. 9B). It is likely that the rates measured on these bedrock samples are representative of a true sample bias; samples of pristine, unweathered bedrock outcrops will yield very low CRN erosion rates, because the surface of the outcrop is neither eroding nor weathering. However, the difference in erosion rate observed between small catchments and bedrock outcrop is something of a surprise. Further sampling of pristine bedrock, weathered bedrock, and detrital samples over small catchments will be necessary to determine the implications of the erosion rates measured from each of these types of sample on the denudation history of the landscape.

5. Discussion and conclusions

We have presented a numerical simulation for modeling the production, decay, and distribution of cosmogenic nuclides on a landscape, and their removal through bedrock weathering and mass wasting processes. Although this simulation was developed to model the effects of landsliding on CRN-derived erosion rates, the framework of the simulation could be adapted to model any number of factors that affect erosion rates derived from CRNs in sediments, including spatial variations in lithology and mineral content, ice cover, annual snowfall, and recent effects of glaciation. In the past, careful researchers trying to exploit CRNs to obtain erosion rates have commonly restricted their sampling to small, unglaciated catchments with uniform lithologies and slow erosion rates. Variations in CRN production due to topographic shielding, slope, lithology, snow and ice cover, and glacial history have generally been ignored. With the ability to numerically predict the effects of such variations, studies can be expanded into larger catchments with higher erosion rates, diverse sediment-production processes, and spatial heterogeneities in CRN concentrations and events that can re-set the cosmogenic clock.

Our landsliding model is underpinned by the observed frequency–magnitude relationships of landslides in two mountain ranges (Southern Alps and

San Gabriel Mountains; [16,17]. These happen to yield nearly identical exponential scaling factors ($\beta = 1.1$) that imply that large, infrequent landslides dominate the total sediment flux. The observation that implementation of our frequency–magnitude-based landsliding module yields volumetric rates that oscillate around the expected value suggests that the model succeeds in mimicking a natural process. This frequency–magnitude relationship and the appropriate scaling factor need to be verified in other mountain ranges before they are routinely applied. In addition, we make the implicit assumption that all of the sediment generated by a landslide is delivered and homogeneously mixed with bedrock weathering-derived sediment within a single model time step (100 yr). We make no attempt to model sediment storage on hillslopes or within fluvial systems or to model particle size fractionation between bedrock weathering-derived and landslide-derived debris [38,39].

Our specific evaluation of the effects of bedrock landsliding on erosion rates derived from CRNs using this simulation yielded several results that have been previously described, particularly that stochastic processes, dominated by large rare events, are difficult to measure using basin-averaging sediment-sampling techniques, because the large, rare events will often not be represented in the sample population [39,40]. However, our simulations also indicate that the median CRN-determined erosion rates are representative of the volumetric erosion rates derived from the same catchments. This suggests that sampling multiple, similarly sized catchments, even in active, landslide-dominated mountain belts, offers a significant likelihood of yielding several samples with consistent CRN erosion rates. These rates are likely to be representative of the recent erosion within those catchments, although it must be recognized that such results will typically be lower than the long-term average that includes the large, rare events. As long as spatial variations in production can be adequately accounted for, as is done within our modeling environment, then larger catchments will always yield a better approximation of long-term erosion rate in landslide-dominated terrains than smaller catchments. Although a specific relationship between the catchment size necessary to spatially average CRN samples and erosion rate is difficult to derive, based on our modeling results, a general rule of thumb appears to be

$$A_{\mathrm{avg}} \ \mathrm{km}^2 = \frac{100 \mathrm{km}^3/\mathrm{Myr}}{E \ \mathrm{km}/\mathrm{Myr}} \tag{7}$$

where A_{avg} is the area needed to average the variability in CRN concentration, and E is the estimated erosion rate over the catchment.

Sampling from bedrock outcrops to measure average erosion rates in landslide-dominated catchments, however, is unlikely to be a useful exercise. At the low end of landslide erosion rates, such samples will faithfully yield the bedrock weathering rate on the landscape, but at increased rates of landslide erosion, such samples will only yield a very rough upper bound on the bedrock weathering rate and, more likely, will be uninterpretable in the context of the spatially averaged erosion rate over the study area.

Finally, the response time of [10]Be concentrations over the landscape to changes in rates of erosional processes is thousands to tens of thousands of years. Regions that have undergone recent changes in rates of erosion may yield CRN-derived erosion rates that reflect some intermediate rate between the previous and current erosion rates during the re-establishment of [10]Be equilibrium over the landscape.

Acknowledgements

Appendix A

Governing equations

This appendix details the derivations of three specific portions of the landslide model, calculating

the rate of landsliding, κ, given a mean landslide erosion rate, E_{ls}; population of landslides in model space, and determining mean cosmogenic concentration per volume of material removed from the model.

Rate of landsliding

We assume that landslides follow a power-law frequency–magnitude distribution [7,16]. For such a distribution, the cumulative frequency of landslides can be written as

$$n_{A \geq A_s} = \kappa (A_s / A_r)^{-\beta} A_r, \tag{A1}$$

where $n_{A \geq A_s}$ is the number of landslides greater than area A_s that occur in a given year, A_r is a specified reference area, κ is the rate of landsliding, and β is the power-law exponent of the frequency–magnitude distribution ([7], see Eq. (1)). If A_r is taken to be 1 km^2, then from Eq. (A1), the total number of landslides per year, n, over the reference area can be written as

$$n_r = \int_{A_{min}}^{A_{max}} \kappa A^{-\beta} dA, \tag{A2}$$

$$= \kappa \left(A_{max}^{-\beta} - A_{min}^{-\beta} \right), \tag{A3}$$

where A_{min} is the area of the smallest landslide to occur in A_r (in the case of the simulation, A_{min} is equal to the model cell size) and A_{max} is the largest slide area, constrained by local topographic relief. Because A_{min} and A_{max} can be constrained either empirically or based on physical characteristics of the model space, and β has been shown to be ~1 over a large range of landslide erosion rates [7,16,17], the volume of material removed by landsliding must be controlled by the rate of landsliding, κ. Because we would prefer to prescribe a rate of erosion due to landslides, E_{ls} for the model, we need to solve for κ in terms of E_{ls}. To do this, we start by determining the number of slides, n_{A_s}, of a given area, A_s per year over the reference area, A_r,

$$n_{A_s} - \kappa \beta A_s^{-1-\beta}. \tag{A4}$$

Given this, the volume of erosion in any year due to landslides of area A_s is equal to the number of landslides of area A_s multiplied by the volume of landslides of area A_s,

$$V_{A_s} = \kappa \beta A_s^{-1-\beta} V_s. \tag{A5}$$

In this simulation, we have opted to model the landslides with parabolic cross sections and a linear relationship between maximum slide depth and width [7,41]. The scaling between landslide area and depth is defined by a scaling factor, ε, with an empirically determined value of ~0.05 [7]. For a slide of a given area A_s, then, the maximum landslide depth, d_{max} and radius, r_{max}, are given by

$$d_{max} = \varepsilon \sqrt{A_s} \tag{A6}$$

and

$$r_{max} = \sqrt{\frac{A_s}{\pi}}. \tag{A7}$$

The depth of the landslide, d, at any given radius from the landslide center is a function of d_{max}, the radius, r, and a constant, C,

$$d = d_{max} - Cr^2. \tag{A8}$$

Because $d=0$ at r_{max}, we can solve for C,

$$C = \frac{d_{max}}{r_{max}^2} = \frac{\varepsilon \sqrt{A_s}}{A_s / \pi} = \frac{\varepsilon \pi}{\sqrt{A_s}}, \tag{A9}$$

allowing us to solve for d as a function of A_s,

$$d = \varepsilon \sqrt{A_s} - \frac{\varepsilon \pi}{\sqrt{A_s}} r^2. \tag{A10}$$

The volume, V_s, of a landslide of area A_s can then be calculated by integrating over cylindrical shells from $r=0$ to r_{max},

$$V_s = 2\pi \int_0^{r_{max}} \varepsilon \sqrt{A_s} - \frac{\varepsilon \pi}{\sqrt{A_s}} r^2 r dr \tag{A11}$$

$$= \frac{\varepsilon}{2} A_s^{3/2} \tag{A12}$$

Eq. (A12) can be substituted back into Eq. (A5) to yield the volume of material, V_{A_s}, removed from the reference area, A_r per year by slides of area A_s,

$$V_{A_s} = \frac{1}{2} \kappa \varepsilon \beta A_s^{(1/2 - \beta)}. \tag{A13}$$

The total volume of erosion per year from reference area A_r, then, is the sum of the erosion due to landslides of all sizes that occur in A_r, from A_{min} to A_{max},

$$V_r = \frac{1}{2} \kappa \varepsilon \beta \int_{A_{min}}^{A_{max}} A_{ls}^{(1/2 - \beta)} dA$$

$$= \frac{\kappa \varepsilon \beta}{(3 - 2\beta)} \left(A_{max}^{(3/2 - \beta)} - A_{min}^{(3/2 - \beta)} \right). \tag{A15}$$

The total erosion rate per year due to landslides, then, can be determined by dividing the volume of material eroded per year by landslides over A_r by the area of A_r,

$$E_{ls} = \frac{V_r}{A_r} \tag{A16}$$

and because we have defined A_r to be a unit area (1 km²),

$$E_{ls} = V_r \tag{A17}$$

Thus, Eq. (A15) can be solved for κ in terms of E_{ls} to yield

$$\kappa = \frac{E_{ls}(3 - 2\beta)}{\varepsilon \beta \left(A_{max}^{(3/2 - \beta)} - A_{min}^{(3/2 - \beta)} \right)}. \tag{A18}$$

Substituting Eq. (A18) into Eq. (A3) yields the total number of landslides, n_r, per year over the reference area, A_r, in terms of known or prescribed values A_{min}, A_{max}, β, ε, and E_{ls},

$$n_r = \frac{E_{ls}(3 - 2\beta) \left(A_{max}^{-\beta} - A_{min}^{-\beta} \right)}{\varepsilon \beta \left(A_{max}^{(3/2 - \beta)} - A_{min}^{(3/2 - \beta)} \right)} \tag{A19}$$

The total number of landslides, n_{ls}, then, in the simulation for a given time step, t, over the entire simulation is

$$n_{ls} = t \times n_r \times \frac{A_{sim}}{A_r} \tag{A20}$$

where A_{sim} is the area, in km², of the simulation.

Landslide population and distribution

With the number of landslides per time step determined, the simulation is populated. The position each landslide is specified by a randomly generated x,y coordinate pair. The size of a given landslide is derived from the landslide frequency–magnitude relationship (Eq. (A1)). The probability of a landslide with area A_s occurring is

$$P_{A_s} = \kappa A_s^{-\beta} \tag{A21}$$

therefore, randomly generated numbers mapped linearly onto the range $P_{A_{min}}$ to $P_{A_{max}}$ can be used to create a population of n_{ls} landslides that fit the frequency–magnitude distribution $\kappa A^{-\beta}$.

Cosmogenic nuclide concentration in eroded material

For each model step, the total depth of material removed from a given cell, D, is the sum of material eroded by bedrock weathering, E_b and the material eroded by landslides, E_{ls}. Using the surface concentration of a cosmogenic nuclide at the end of the model step, $N_f^{10}Be$, the average nuclide concentration in the volume of eroded material, $N_D^{10}Be$ can be calculated by integrating over the total depth of eroded material the concentration of the nuclide as a function of e-folding depth, Λ,

$$N_D^{10}Be = N_f^{10}Be \cdot \rho \int_{-D}^{0} e^{-z(\rho/\Lambda)} dz \tag{A22}$$

$$= N_f^{10}Be \cdot \Lambda \left(e^{D(\rho/\Lambda)} - 1 \right). \tag{A23}$$

References

[1] P. Molnar, P. England, Late Cenozoic uplift of mountain ranges and global climate change: chicken or egg? Nature 346 (1990) 29–34.

[2] E.T. Brown, R.F. Stallard, M.C. Larsen, G.M. Raisbeck, F. Yiou, Denudation rates determined from the accumulation of in situ produced [10]Be in the Luquillo experimental forest, Puerto Rico, Earth Planet. Sci. Lett. 129 (1995) 193–202.

[3] P. Bierman, E.J. Steig, Estimating rates of denudation using cosmogenic isotope abundances in sediment, Earth Surf. Processes Landf. 21 (1996) 125–139.

[4] D.E. Granger, J.W. Kirchner, R. Finkel, Spatially averaged long-term erosion rates measured from in situ produced cosmogenic nuclides in alluvial sediments, J. Geol. 104 (1996) 249–257.

[5] E.M. Clapp, P.R. Bierman, A.P. Schick, J. Lekach, Y. Enzel, M. Caffee, Sediment yield exceeds sediment production in arid region drainage basins, Geology 28 (2000) 995–998.

[6] C.S. Riebe, J.W. Kirchner, D.E. Granger, R.C. Finkel, Erosional equilibrium and disequilibrium in the Sierra Nevada, inferred from cosmogenic ^{26}Al and ^{10}Be in alluvial sediment, Geology 28 (2000) 803–806.

[7] N. Hovius, C.P. Stark, P.A. Allen, Sediment flux from a mountain belt derived by landslide mapping, Geology 25 (1997) 231–234.

[8] A.M. Heimsath, C. Wobus, Erosion rates and processes across two trans-Himalayan transects in central Nepal, Eos, Trans.-Am. Geophys. Union 85 (2004) (Abstract T3B4-03).

[9] A. Heimsath, Eroding the Himalaya: pushing the limits of cosmogenic nuclides, 32nd Int. Geol. Congr. electronic version posted on-line on July 20, 2004, Abs. Vol., pt. 1 (2004) Abs. 196-7.

[10] S.A. Binnie, J.A. Spotila, W.M. Phillips, M.A. Summerfield, K.A. Fifield, The coexistence of steady and non-steady state topography in the San Bernardino Mountains, southern California, from cosmogenic ^{10}Be and UTh/He thermochronology, Geol. Soc. Am., Abstr. Prog. 35 (2003).

[11] T.J. Dunai, Scaling factors for production rates of in situ produced cosmogenic nuclides; a critical reevaluation, Earth Planet. Sci. Lett. 176 (2000) 157–169.

[12] T.J. Dunai, Erratum to Scaling factors for production rates of in situ produced cosmogenic nuclides; a critical reevaluation, Earth Planet. Sci. Lett. 178 (2000) 425.

[13] A. Dunne, D. Elmore, P. Muzikar, Scaling factors for the rates of production of cosmogenic nuclides for geometric shielding and attenuation at depth on sloped surfaces, Geomorphology 27 (1999) 3–11.

[14] J. Masarik, R.C. Reedy, Terrestrial cosmogenic-nuclide production systematics calculated from numerical simulations, Earth Planet. Sci. Lett. 136 (1995) 381–395.

[15] A. Heimsath, The soil production function, PhD, University of California, 1999.

[16] C.P. Stark, N. Hovius, The characterization of landslide size distributions, Geophys. Res. Lett. 28 (2001) 1091–1094.

[17] J. Lavé, D. Burbank, Denudation processes and rates in the Transverse Ranges, Southern California; erosional response of a transitional landscape to external and anthropogenic forcing, J. Geophys. Res. 109 (2004) 31.

[18] F. Guzzetti, B.D. Malamud, D.L. Turcotte, P. Reichenbach, Power-law correlations of landslide areas in central Italy, Earth Planet. Sci. Lett. 195 (2002) 169–183.

[19] B.D. Malamud, D.L. Turcotte, F. Guzzetti, P. Reichenbach, Landslide inventories and their statistical properties, Earth Surf. Processes Landf. 29 (2004) 687–711.

[20] E.L. Harp, R.W. Jibson, Inventory of Landslides Triggered by the 1994 Northridge, California Earthquake, Tech. Rep., U.S. Geological Survey, Reston, VA, United States (USA), 1995.

[21] Y. Fuyii, Frequency distribution of the magnitude of landslides caused by heavy rainfall, J. Seismol. Soc. Jpn. 22 (1969) 244–247.

[22] N. Hovius, C.P. Stark, C. Hao-Tsu, L. Jinn-Chaun, Supply and removal of sediment in a landslide-dominated mountain belt; Central Range, Taiwan, J. Geol. 108 (2000) 73–89.

[23] O. Hungr, S.G. Evans, J. Hazzard, Magnitude and frequency of rock slides along the main transportation corridors of southwestern British Columbia, Can. Geotech. J. 36 (1999) 224–238.

[24] D. Lal, Cosmic ray labeling of erosion surfaces; in situ nuclide production rates and erosion models, Earth Planet. Sci. Lett. 104 (1991) 424–439.

[25] D.E. Granger, P.F. Muzikar, Dating sediment burial with in situ produced cosmogenic nuclides: theory, techniques, and limitations, Earth Planet. Sci. Lett. 188 (2001).

[26] A.E. Blythe, D.W. Burbank, K.A. Farley, E.J. Fielding, Structural and topographic evolution of the central Transverse Ranges, California, from apatite fission-track, (U–Th)/He and digital elevation model analyses, Basin Res. 12 (2000) 97–114.

[27] A.E. Blythe, M.A. House, J.A. Spotila, Low-temperature thermochronology of the San Gabriel and San Bernardino mountains, southern California; constraining structural evolution, in: A. Barth (Ed.), Contributions to Crustal Evolution of the Southwestern United States, Special Paper, vol. 365, Geological Society of America, 2002, pp. 231–250.

[28] J.A. Spotila, M.A. House, A.E. Blythe, N.A. Niemi, G.C. Bank, Controls on the erosion and geomorphic evolution of the San Bernardino and San Gabriel mountains, southern California, in: A. Barth (Ed.), Contributions to Crustal Evolution of the Southwestern United States, Special Paper, vol. 365, Geological Society of America, 2002, pp. 205–230.

[29] D.M. Morton, F.K. Miller, Preliminary geologic map of the San Bernardino 30′ × 60′ quadrangle, California, Open-File Report, vol. 03-293, U.S. Geological Survey, 2003.

[30] M. Julian, E. Anthony, Aspects of landslide activity in the Mercantour massif and the French Riviera, southeastern France, Geomorphology 15 (1996) 175–289.

[31] J.F. Shroder, Mass movement in the Himalaya: an introduction, Geomorphology 26 (1998) 9–11.

[32] W.B. Bull, Geomorphic Responses to Climatic Change, Oxford University Press, Oxford, 1991.

[33] D.W. Burbank, A.E. Blythe, J. Putkonen, B. Pratt-Sitaula, E. Gabet, M. Oskin, A. Barros, T.P. Ojha, Decoupling of erosion and precipitation in the Himalayas, Nature 426 (2003) 652–655.

[34] E.J. Gabet, D.W. Burbank, J.K. Putkonen, B.A. Pratt-Sitaula, T. Ohja, Rainfall thresholds for landsliding in the Himalayas of Nepal, Geomorphology 63 (2004) 131–143.

[35] B. Pratt-Sitaula, M. Garde, D.W. Burbank, M. Oskin, A.M. Heimsath, E.J. Gabet, Bedload ratio, regional erosion rate, and rapid bedrock incision from Himalayan landslide-dam lake record, Quat. Res. (in press).

[36] J.M. Chambers, W.S. Cleveland, B. Kleiner, P.A. Tukey, Graphical Methods for Data Analysis, Wadsworth, 1983.

[37] J.-C. Chang, O. Slaymaker, Frequency and spatial distribution of landslides in a mountainous drainage basin: western Foothills, Taiwan, Catena 46 (2002) 285–307.

[38] L. Benda, T. Dunne, Stochastic forcing of sediment supply to channel networks from landsliding and debris flow, Water Resour. Res. 33 (1997) 2849–2863.

[39] L. Benda, T. Dunne, Stochastic forcing of sediment routing and storage in channel networks, Water Resour. Res. 33 (1997) 2865–2880.

[40] J.W. Kirchner, R.C. Finkel, C.S. Riebe, D.E. Granger, J.L. Clayton, J.G. King, W.F. Megahan, Mountain erosion over 10 yr, 10 k.y., and 10 m.y. time scales, Geology 29 (2001) 591–594.

[41] H. Ohmori, Morphological characteristics of the scar created by large-scale rapid mass movement, Chikei Trans.–Jpn. Geomorphol. Union 13 (1992) 185–202.